

Optical Engineering

OpticalEngineering.SPIEDigitalLibrary.org

Highly efficient deterministic polishing using a semirigid bonnet

Chunjin Wang
Wei Yang
Zhenzhong Wang
Xu Yang
Zhiji Sun
Bo Zhong
Ri Pan
Ping Yang
Yinbiao Guo
Qiao Xu

Highly efficient deterministic polishing using a semirigid bonnet

Chunjin Wang,^{a,b} Wei Yang,^{a,*} Zhenzhong Wang,^a Xu Yang,^{a,b} Zhiji Sun,^{a,b} Bo Zhong,^c Ri Pan,^a Ping Yang,^a Yinbiao Guo,^a and Qiao Xu^b

^aXiamen University, Department of Mechanical and Electrical Engineering, Xiamen 361005, China

^bChina Academy of Engineering Physics, Research Center of Laser Fusion, Mianyang 621900, China

^cFine Optical Engineering Research Center, Chengdu 610041, China

Abstract. This paper presents a semirigid (SR) bonnet tool which has the advantages of high efficiency and determinacy for material removal on optical elements and also has the potential to be used on aspheric optics. It consists of three layers: a metal sheet, a rubber membrane, and a polishing pad, from inside to outside. It inherits the flexibility of a normal bonnet but has a higher stiffness. Finite element analysis was performed to determine that the stainless steel is the best-suited material for use as the metal sheet. An SR bonnet with a stainless-steel metal sheet was fabricated and tested. Its tool influence function (TIF) is Gaussian-like, and the TIF stability is more than 90%. The peak-to-valley of its uniform removal area is less than 0.1λ . Tool ripples are highly depressed and the surface profile is well preserved in the prepolishing test. In 12 min, $\sim 36 \text{ mm}^3$ of material is removed. © The Authors. Published by SPIE under a Creative Commons Attribution 3.0 Unported License. Distribution or reproduction of this work in whole or in part requires full attribution of the original publication, including its DOI. [DOI: 10.1117/1.OE.53.9.095102]

Keywords: deterministic polishing; semirigid bonnet; bonnet polishing; aspheric optics.

Paper 140769 received May 13, 2014; revised manuscript received Jul. 24, 2014; accepted for publication Aug. 15, 2014; published online Sep. 9, 2014.

1 Introduction

When used in an optical system, aspheric optics can increase the degrees-of-freedom (DOF) in a design, reduce the system's weight and size, and provide a significant advantage for correcting system aberrations.¹ When using traditional polishing methods, the production of aspherics, especially in the polishing stage, involves several challenges such as the mismatch between the tool-surface and the work-piece, the dependency on skilled workers, the unpredictability of removal, inefficiency, and so on. Therefore, various computer-controlled optical surfacing (CCOS) processes have been developed since the 1960s.²⁻⁷ Jones⁸ successfully adopted a small-pitch-tool approach with their CCOS facility for large optics, but its removal efficiency remained low and there was an obvious edge effect. Kodak⁹⁻¹⁰ reported results on ion beam figuring (IBF) technology, which can achieve an extra-high-precision surface. However, it is well known that this technology's material removal efficiency is particularly low. Fluid jet polishing, which is similar to IBF, was developed by Fähnle et al.¹¹ In the 1990s, Kordonski et al.¹² proposed a magnetorheological finishing process, which demonstrates a high level of predictability but is not effective for removing mid-spatial frequency errors.

A bonnet polishing technology adopting the precession movement (called "bonnet polishing" for brief) was developed by Zeeko Ltd. (Leicestershire, United Kingdom) in collaboration with the Optical Science Laboratory at the University College London and Loh Optikmaschinen.^{13,14} This technology uses a rotating inflated spherical membrane tool (the "bonnet"), which naturally molds itself to the local aspheric surface and maintains stability to provide natural smoothing. Compared to other polishing processes, the

bonnet shows higher removal efficiency, excellent removal of mid-spatial frequencies, and the ability to control the mirror's edges.¹⁵⁻¹⁹ A bonnet has thus been widely used for polishing optical lenses, especially aspherics,²⁰ molds,²¹ freeform surfaces,²² structured surfaces,²³ and so on.

Bonnet polishing can deliver higher removal rates than the aforementioned polishing processes. Nevertheless, the rate is not sufficiently high for large parts or for parts with large form errors. When encountering large errors, the compliant bonnet would follow the surface down into the depression. Consequently, the grooving process was developed, which is intermediate between grinding and polishing.²⁴ This process can make the surface converge rapidly with reasonable accuracy. But the surface after grooving exhibits substantial subsurface damage, and the depth of this damage is close to or even deeper than that of the surface after precision grinding.²⁵ In addition, the grooving process is unpredictable, and the manufacture of its tool is complicated.

The present work introduces a semirigid (SR) bonnet polishing tool, which is proven to have a far higher removal rate than the normal bonnet. Its removal function is near-Gaussian and has excellent stability. Consequently, the SR bonnet polishing tool may offer an attractive solution for prepolishing large aspheric mirrors or mirrors with large form errors, and the tool also has the potential to perform corrective polishing.

2 Theoretical Background

Bonnet polishing is a newly developed type of subaperture polishing. The tool comprises a spinning inflated bulging rubber membrane with a spherical form. This tool is covered with a polishing cloth (often composed of polyurethane) and operates in the presence of a cerium oxide polishing slurry. The bonnet is brought into contact with the surface to be

*Address all correspondence to: Wei Yang, E-mail: yangwei@xmu.edu.cn

polished and then compresses to create a defined polishing spot.¹³ The orientation of the tool-rotation axis can be controlled at a defined inclination angle with respect to the local normal surface over the entire work-piece. The tool axis is then processed in (typically four) discrete steps about the local-normal to the part's surface. This process generates an accumulated influence function which is near-Gaussian.¹⁴

The material removal function $D(r)$ for bonnet polishing is derived from the well-known Preston equation, expressed as

$$D(r) = k \cdot P(r) \cdot V(r), \quad (1)$$

where k is the Preston constant, $P(r)$ is the pressure distribution in the contact area, $V(r)$ is the relative speed between the tool and the work-piece surface, and r is the radial distance from the center of the contact area. If k and $V(r)$ remain unchanged, the form of $D(r)$ is dominated by pressure distribution $P(r)$. A larger $P(r)$ would deliver a deeper $D(r)$. Due to the flexibility of the rubber membrane, the tool can conform to the aspheric shape, but lacking intrinsic stiffness, the tool can only generate limited pressure. Consequently, changing the structure of the bonnet to achieve higher stiffness and maintain conformability to aspheric surface would be a reasonable means of realizing highly efficient polishing.

3 Design of the Tool

3.1 Structure of the SR Bonnet

A normal bonnet tool can easily conform to the aspheric or freeform surface, but its material removal rate is not that high due to low contact pressure. Also, the spherical tool contour turns into aspheric under the effect of regular inner pressure

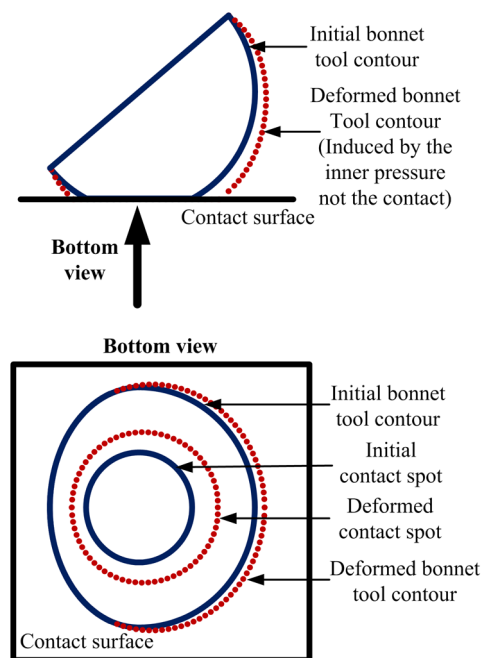


Fig. 1 Schematic diagram of the effect of bonnet tool deformation to the contact spot. The initial bonnet tool has a spherical shape. Under the effect of the inner pressure, the bonnet contour deformed to aspheric shape as shown in the left part of the figure. Also, if the tool contour is spherical, the shape of the contact spot would be a standard circle. But due to the effect of the tool deformation, the contact spot shape becomes irregular.

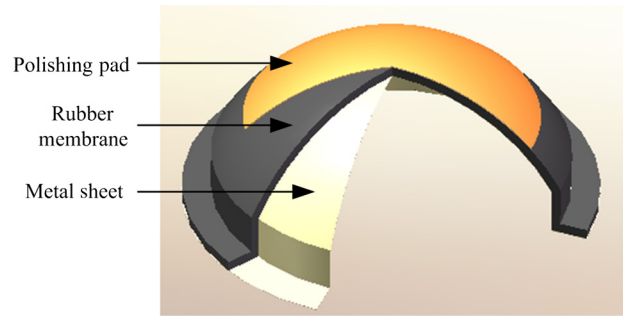


Fig. 2 Structure of the semirigid (SR) bonnet.

as shown in Fig. 1. This makes it difficult to control the contact spot shape and make the tool setting process fussy.

To enhance the stiffness of the bonnet and maintain a certain flexibility, we embed a thin metal sheet—which has been shaped to fit the inner surface—into the rubber membrane. Figure 2 shows the structure of the SR bonnet. There are three layers stuck together, and from the bonnet's interior to its exterior, those layers are the following: the metal sheet, the rubber membrane, and the polishing pad. The metal sheet has high stiffness, but due to its thinness, the metal sheet is suitably flexible. Combined with the highly flexible rubber membrane, the metal sheet results in an SR bonnet tool.

3.2 Determination of the Metal Sheet Material Using the FEA Method

The metal sheet can be shaped from common metal materials, such as stainless steel, copper, aluminum, and so on. However, to perfect the SR bonnet, choosing the material that exhibits the best properties is critical. The mold to form the metal sheet is sufficiently expensive that it is unrealistic to make three different molds for the experiment to determine the best material. Therefore, the finite element analysis (FEA) method is adopted. Our purpose is to analyze the distribution and magnitude of the metal sheet pressure and deformation under the same inner pressure. A group of simulation experiments is conducted using three different materials as the metal sheet: stainless steel, copper, and aluminum. Li et al.¹⁹ had built the FEA model for a normal bonnet polishing a Zerodur part, and they used this model to determine the pressure distribution in the contact area. To simplify the problem, the polishing pad is neglected in the model.¹⁹ Hence, we also build a simulation model omitting the effect of the polishing pad. A BK7 part—whose size is $50 \times 50 \text{ mm}^2$ and whose thickness is 5 mm—is used in the simulation. Table 1 lists the material properties for this model, and the simulation conditions are shown in Table 2.

Figure 3 shows the simulation model for the SR bonnet polishing the BK7 part. Figure 3(a) is the model adopted to simulate the deformation under the effect of inner pressure. The top surface of the bonnet is constrained with zero displacement in all directions. The inner pressure and the symmetric constraint are also applied at the same spot as in the previous discussion. Figure 3(b) is the model used to simulate the pressure distribution over the contact area. The spherical part of the bonnet tool is used to simplify the simulation model. Considering the model's symmetry, half of the model is adopted to enhance the solution's efficiency. All DOF for the work-piece's bottom surface are constrained with zero displacement. The top surface of the SR bonnet is

Table 1 Material characteristics for model.

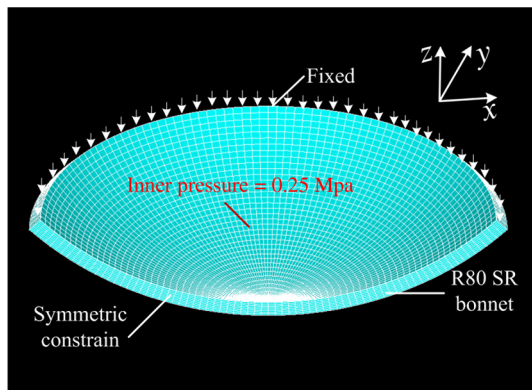
Material	Density (kg/m ³)	Young's modulus (Mpa)	Poisson's ratio
Synthetic rubber	0.95E + 3	1.5	0.47
BK7	2.51E + 3	8.1E + 4	0.206
Stainless steel	7.30E + 3	1.9E + 5	0.26
Copper	8.96E + 3	1.1E + 5	0.35
Aluminum	2.70E + 3	6.8E + 4	0.36

Table 2 Simulation conditions.

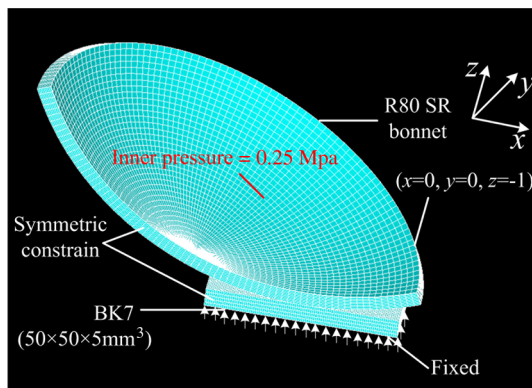
Tool size ^a (mm)	Inner pressure (Mpa)	Precession angle (deg)	Z-offset ^b
R80	0.25	23	1

^aThe rubber layer's thickness is 3.5 mm, and the metal sheet is 0.2 mm in thickness.

^bZ-offset is the displacement of the tool's nadir toward to the work-piece.



(a)



(b)

Fig. 3 (a) Model to simulate bonnet deformation under the effect of inner pressure and (b) simulation model of the SR bonnet polishing the BK7 part.

constrained with zero displacement along the x -axis and y -axis with a -1 -mm displacement along the z -axis. The inner pressure is applied on the bonnet's inner surface. The symmetric constraint is applied on the symmetrical section.

Figure 4 shows the simulation results for both the pressure distribution and the deformation of different SR bonnets. Figures 4(a) and 4(b) are the simulation results for the SR bonnet with a stainless steel metal sheet. Figures 4(c) and 4(d) show the simulation results for the SR bonnet with a copper metal sheet. The simulation results for the SR bonnet with an aluminum metal sheet are shown in Figs. 4(e) and 4(f). The deformation under the effect of the inner pressure of the SR bonnet with the stainless steel metal sheet is the smallest ($17 \mu\text{m}$), and it also can deliver the largest contact pressure (1.327 MPa) among all three materials. Additionally, there is a discontinuous pressure distribution along the contact area's edge when the metal sheet material is copper or aluminum as shown in Figs. 4(d) and 4(f). This discontinuity mainly results when the z -offset reaches 1 mm, and the SR bonnet with a copper or aluminum metal sheet experiences inward-concavity. Larger contact pressure could deliver a higher material removal rate, and the bonnet deformation under the effect of inner pressure is adverse for controlling the size of the contact spot as explained in Fig. 1. Therefore, among all three materials, stainless steel is the superior metal sheet material.

To specifically analyze the contact pressure distribution, the contact pressure on the section line of each simulation result has been extracted and fitted using the following Gaussian-like equation.²⁶

$$P = P_T \left[\exp\left(-\frac{x^2}{2\sigma^2}\right) \right]^\psi, \quad (2)$$

where P is the contact pressure, P_T is the maximum contact pressure, σ is the standard deviation, and ψ is the modification coefficient. The fitting results for different SR bonnets with different metal sheet materials are displayed in Fig. 5.

Note that the maximum contact pressure delivered by the SR bonnet is much larger than the R160 normal bonnet (mentioned in Fig. 7 in Sec. 3.3 of Ref. 19), whose maximum contact pressure is 0.117 Mpa. Hence, the SR bonnet would generate higher material removal efficiency than the normal bonnet. Furthermore, the SR bonnet's deformation is much smaller than the normal bonnet's deformation, which is at the same level of polishing as the machine's accuracy, and thus the deformation error of the tool contour can be ignored during the polishing process, while the shape of the contact spot can be considered to be a standard circle. Therefore, the size of the contact spot can be accurately controlled by controlling the z -offset.

3.3 Determination of the Thickness of Stainless Steel Sheet

The designed thickness of the stainless steel sheet is crucial for the property of the SR bonnet. Therefore, we also conduct five groups of simulation experiments using five different thicknesses for the steel sheet, which are 0.1, 0.15, 0.2, 0.25, and 0.3 mm, respectively. The simulation conditions are the same as previously mentioned. Both the SR bonnet deformation under the effect of inner pressure is simulated using the model as shown in Fig. 3(a) and the bonnet

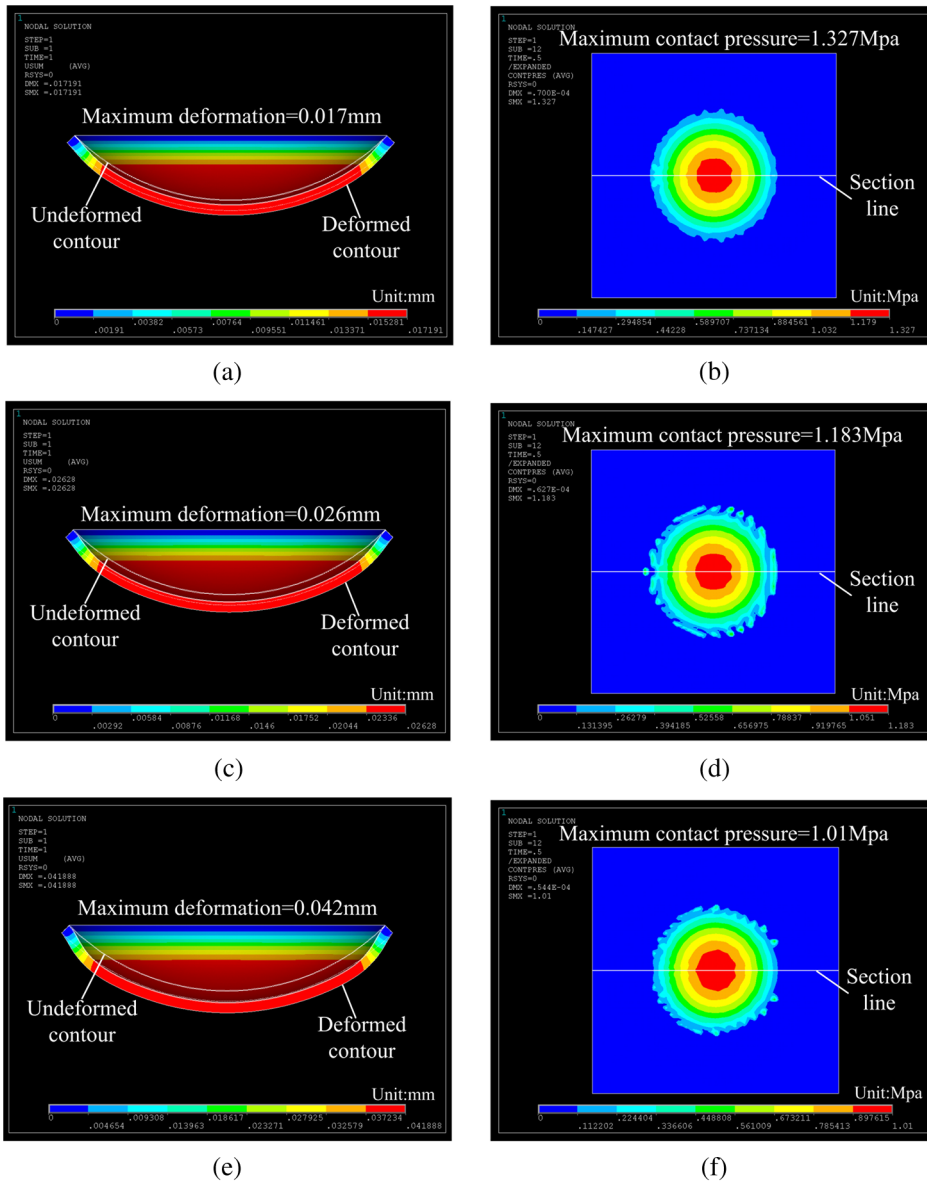


Fig. 4 (a) Bonnet deformation when the metal sheet material is stainless steel, (b) contact pressure distribution when the metal sheet material is stainless steel, (c) bonnet deformation when the metal sheet material is copper, (d) contact pressure distribution when the metal sheet material is copper, (e) bonnet deformation when the metal sheet material is aluminum, and (f) contact pressure distribution when the metal sheet material is aluminum. * In order to see the deformation clearly, the deformation has been scaled 100 times.

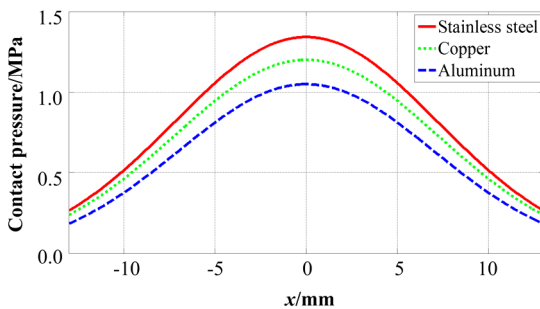


Fig. 5 Pressure distribution on the section line of different SR bonnets with different metal sheet materials.

tool compress to the work-piece is simulated adopting the model as shown in Fig. 3(b).

The simulation results have been shown in Fig. 6. Figure 6(a) shows the deformation of the SR bonnet tool under the effect of the inner pressure that varies with the thickness of the stainless steel sheet together with the maximum contact pressure curve. A thicker sheet will lead to a higher stiffness. This results in less deformation of the tool and a larger maximum contact pressure. The maximum von Mises stress of the tool during the tool compress to the work-piece surface is also extracted and compared to the yield limit stress of the stainless steel as shown in Fig. 6(b). It is noted that when the thickness is 0.1 or 0.15 mm, the maximum von Mises stress is larger than the yield limit, which means that the stainless steel sheet of the SR bonnet will fail to return to

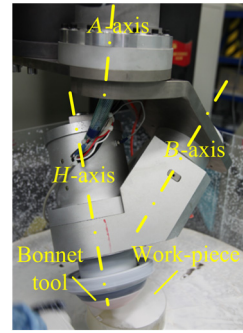
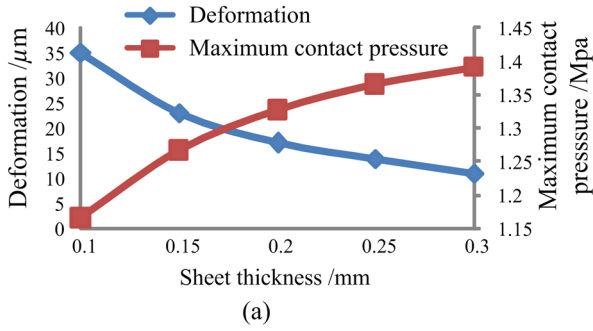


Fig. 8 Experimental prototype for testing the SR bonnet.

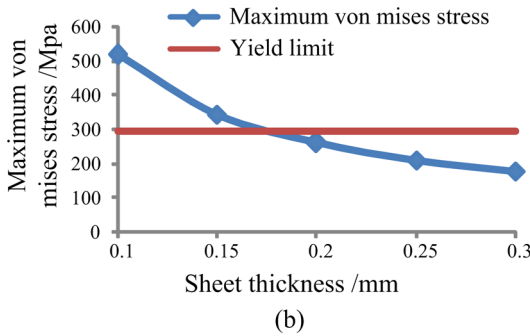


Fig. 6 (a) The deformation of the SR bonnet tool under the effect of the inner pressure and the maximum contact pressure in each result varying with the thickness of the stainless steel sheet, and (b) the maximum von Mises stress in each result vary with the thickness of the stainless steel sheet.

the original shape. Therefore, these two kinds of thicknesses are not appropriate. But when the thickness of this sheet is too large, the SR bonnet will lose flexibility. In order to maintain a certain flexibility of the SR bonnet, 0.2 mm is finally chosen as the thickness of the stainless steel sheet based on the analysis above.

4 Performance of the SR Bonnet Polishing Tool

4.1 Tool Influence Function (TIF) of the SR Bonnet Tool

Through the aforementioned analysis, we have chosen stainless steel with a thickness of 0.2 mm as the material of the metal sheet for the R80 SR bonnet. It has been manufactured as shown in Fig. 7. Figure 8 displays the experimental

prototype designed by our group to test the performance of the SR bonnet. As shown in Fig. 8, the *H*-axis controls the tool rotation of the bonnet tool, the *B*-axis controls the angle between the tool rotation axis and the normal line of the polished surface, and the *A*-axis is designed to make the tool can implement precession motion. In order to observe both its TIF and its TIF stability, a group of experiments to extract four TIFs have been conducted. We use the R80 SR bonnet to polish a BK7 work-piece. The speeds of the *H*-axis and *A*-axis are 500 and 20 rpm, respectively. Cerium oxide slurry (whose weight percentage is 5.54%) is used in the experiment. The dwell time on each



Fig. 7 Picture of the R80 SR bonnet.

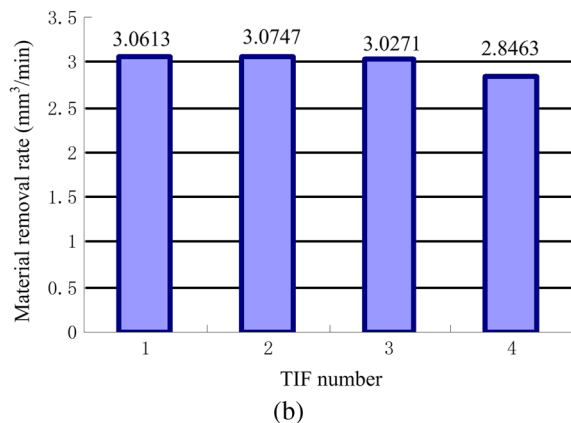
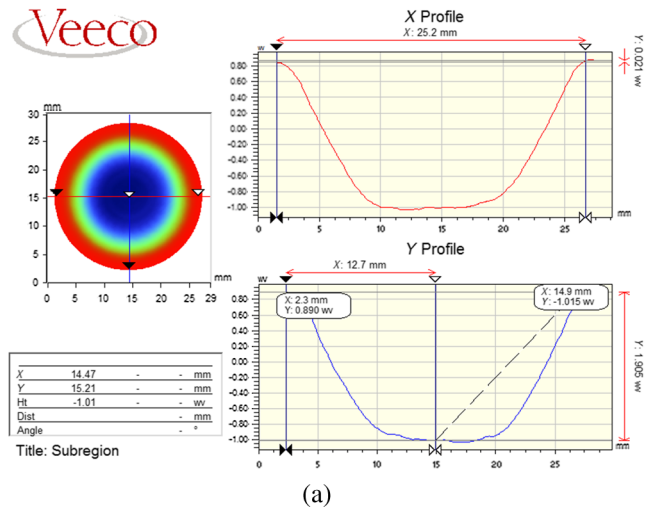


Fig. 9 (a) Extracted shape of tool influence function (TIF) and (b) material removal rate of four TIFs.

spot is 6 s. All other experimental conditions are identical to the conditions listed in Table 2.

Results are presented in Fig. 9. Figure 9(a) shows one TIF of the SR bonnet tool. Its shape is the same as the normal bonnet's shape, which is also a Gaussian-like profile.⁵ Figure 9(b) presents the material removal rate of the four TIFs. As shown in Fig. 9(a), the maximum removal depth is 1.95λ ($\lambda = 632.8$ nm) and the dwell time is only 6 s. In Fig. 9(b), the time between each sample is ~15 min, and the removal rate stability is more than 90%.

In addition, a series of polishing spots with different contact sizes have also been generated on a BK7 part. The extracted spot contours have been demonstrated in Fig. 10. Figure 10(a) shows the extracted contour of six different polishing spots. Their diameters are 14, 20, 25, 28, 30, and 36 mm, respectively. Figure 10(b) shows the section contour of these spots. It turns out that a "W" shape of TIF comes out when the diameter of the spot is over 25 mm. This performance is just like the normal bonnet²⁷ and the size of the spot could not exceed the certain limit.

4.2 Uniform Removal Test

The previous section has demonstrated the SR bonnet's TIF stability. However, stability during the polishing process must also be tested before this tool is put into production. Hence, a uniform removal test of the SR bonnet on the BK7 work-piece has also been conducted. This test is carried out on a plane Φ 120-mm BK7 glass whose surface has been

Table 3 Uniform removal conditions.

Polishing parameters	Value
Tool radius (mm)	80
Precession angle (deg)	23
H-axis speed (rpm)	500
Feed speed (mm/min)	600
Z-offset (mm)	0.7
Inner pressure (Mpa)	0.25
Polishing time (min)	4 each cycle
Slurry weight percentage (%)	1.8

polished to 0.18λ peak-to-valley (p-to-v). In order to leave unpolished surfaces from which an absolute removal depth could be established, a Φ 80-mm subarea of the part was polished. The Z-shaped raster path is used, and the polishing cycle has been executed four times with the precession angle orientated in four polar directions along

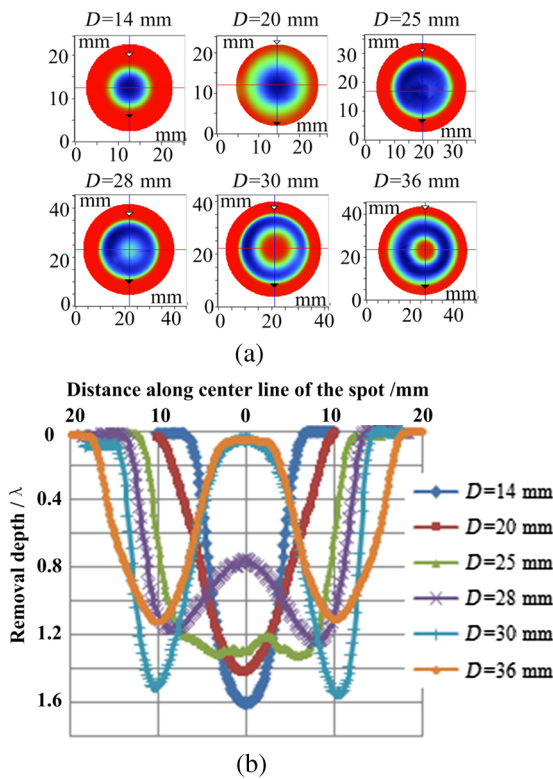


Fig. 10 (a) Contours of the extracted polishing spots with different spot diameters, and (b) section line of each polishing spot. The polishing conditions are as follows: tool radius is 80 mm, precession angle is 23 deg, inner pressure is 0.2 MPa, H-axis rotation speed is 500 rpm, A-axis rotation speed is 20 rpm, and dwell time is 6 s. (D signifies the diameter of the spot, $\lambda = 632.8$ nm).

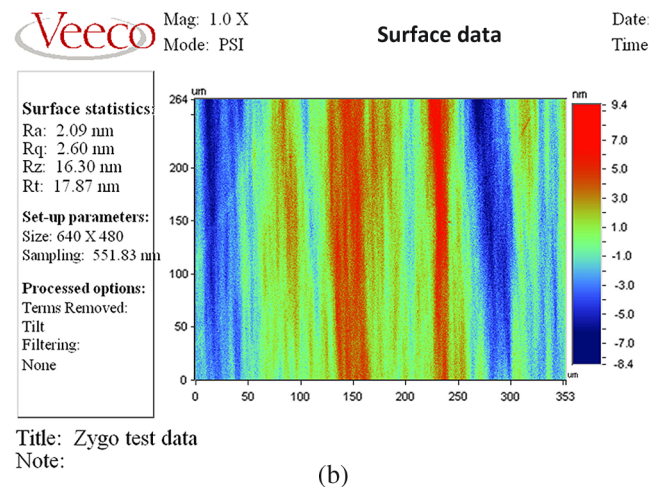
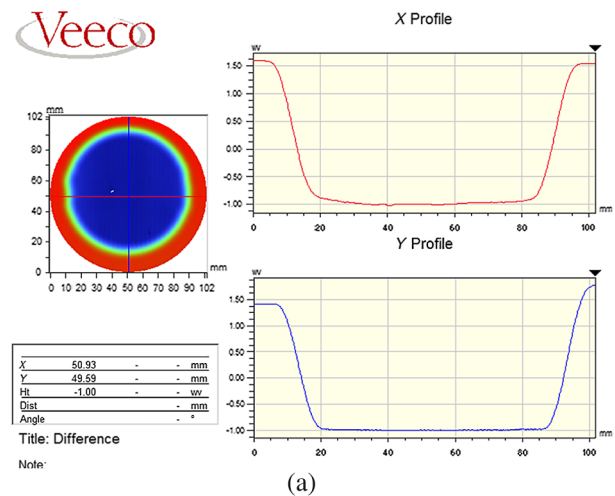


Fig. 11 (a) The whole surface contour after uniform removal polishing and (b) the surface roughness measuring result.

the local normal (0, 90, 180, and 270 deg).⁵ The raster distance is 1.5 mm. Table 3 shows the other experimental conditions.

The experimental results are presented in Fig. 11. Figure 11(a) shows the whole surface contour after uniform removal polishing using the R80 SR bonnet, as measured using QED SSI™. The result demonstrates high uniformity, and the p-to-v of the uniform removal area is less than 0.1λ. Figure 11(b) shows the surface roughness result measured using Zygo (Middlefield, Connecticut) NewView 7200. Its Ra is only 2.09 nm after one cycle of the uniform removal process.

4.3 Prepolishing Test

This process is intended to remove surface and subsurface damage on a part from a precision grinding machine and also to preserve the profile. Typically, material must be removed to a depth of tens of microns. Therefore, a polishing tool with a high removal rate is urgently needed for this process.

The prepolishing test of the SR bonnet has been performed on a BK7 glass. To leave an unpolished region for defining absolute removal, a 60 × 60-mm² area out of a 100 × 100-mm² surface is polished. A Z-shaped raster path is also adopted, and the precession angle is again

orientated in four directions during the entire process. The weight percentage of the cerium oxide in the slurry is 3.04%, and the *H*-axis speed is 750 rpm. Other process conditions are identical to the conditions shown in Table 3. The total prepolishing time is 12 min.

Figure 12(a) shows the initial surface profile after removal from the grinding machine (whose p-to-v is ~3.5 μm), on which obvious tool ripples exist. The profile after the prepolishing process is shown in Fig. 12(b). In 12 min, ~36 mm³ of material are removed and tool ripples are highly depressed.

5 Discussion

The property of the SR bonnet polishing plane optics has been demonstrated above. The average material removal rate of an R80 SR bonnet reaches 3.002 mm³/min as shown in Fig. 9(b), which is much higher than the rate of the normal bonnet.^{27,28} Its high removal rate also can be found in the prepolishing test result, in which ~36 mm³ of material are removed in 12 min. Therefore, the SR bonnet can be adapted to execute a high efficiency polishing.

It is noted in the results of the TIF test and uniform removal test that the stability of the SR bonnet's material removal is quite high both for the TIF itself and during the polishing process. Its TIF is also a Gaussian-like shape and is quite deterministic, which is the same as the

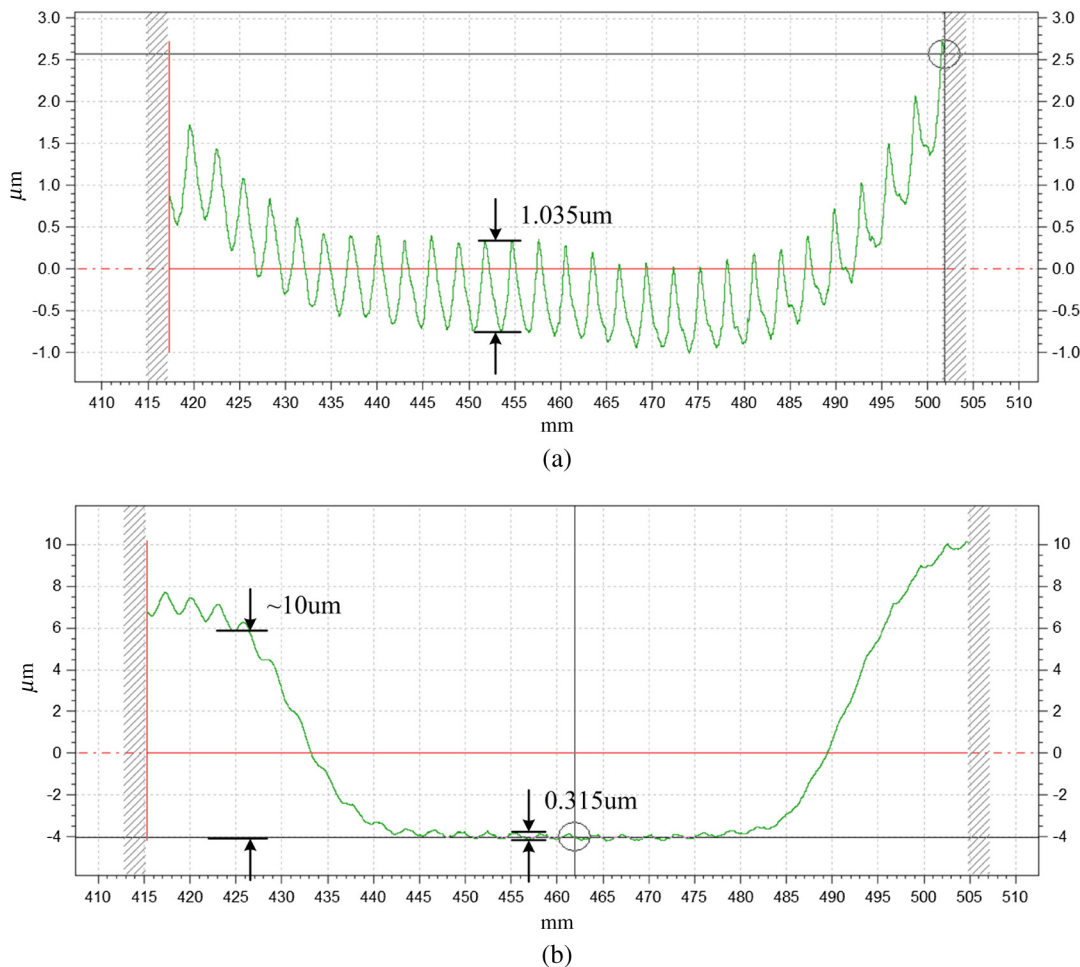


Fig. 12 (a) Profilometry of the part directly off the grinder measured using PGI 1250S Form Talysurf™ and (b) form measured after 12-min prepolish using the R80 SR bonnet.

Table 4 General comparison between different tool types.^{a,b}

	Rigid tool ²⁹	IBF ^{9,30,31}	Magnetorheological finishing ^{12,32}	Fluid jet polishing ^{11,33}	RC lap ²⁹	Normal bonnet ^{5,15}	Semirigid (SR) bonnet
Predictability	Low	Good	Good	Good	Good	Excellent	Excellent
Smoothing	Good	Excellent	Excellent	Good	Medium	Medium	Medium
Removal rate	Low	Low	Medium	Medium	Medium	Good	Excellent
Fitting to aspheric surface	Poor	Good	Good	Good	Good	Good	Good ^c
A tool for different shape of work-pieces	No	Yes	Yes	Yes	Yes	Yes	Yes

Note: Bold items are usually regarded as advantages.

^aThese characteristics are mainly considered when evaluating a polishing tool.

^bThis is just a general comparison. These characteristics may vary for a specific tool.

^cThis is the expected performance based on the semirigid property of the SR bonnet.

normal bonnet. Also, the surface texture of the BK7 material after one cycle of the polishing process can reach $R_a = 2.09$ nm, which is close to the surface texture the normal bonnet can implement (The surface texture of BK7 polished using a normal bonnet can reach $R_a = 2.4$ nm with little difficulty, and the best R_a achieved to date is 0.5 nm.).^{13,14} This experiment was conducted on an experimental prototype with a low accuracy, and a coarse polishing slurry was used whose size is ~ 3 μm . With this in mind, it is believed that the smoothing property of the SR bonnet would be closer to the normal bonnet when these factors are improved. Hence, we deduce that the SR bonnet may have the potential to be used in corrective polishing. The corrective algorithm has not been integrated to the prototype system yet. Therefore, the corrective polishing process using the SR bonnet will be reported in a standalone paper in the future.

The normal bonnet's flexibility is quite high, which makes it conform to an aspheric or freeform surface well, but it cannot be used to diminish the tool ripple left by a grinding machine. As shown in Fig. 12, the tool ripple is highly depressed from p-to-v ~ 1.035 to ~ 0.315 μm with just over one pass of prepolishing and the total profile is well preserved. Combined with its high material removal efficiency, it makes the SR bonnet an attractive solution for prepolishing large mirrors or mirrors with large form errors.

As demonstrated above, all the experiments are implemented on a plane surface and the experiment on the aspheric surface, limited by some objective factors, has not been done. Also, it is found that the removal rate decreases slightly over time which may be induced by the decrease of slurry weight percentage in the prototype. These problems will be handled when the machine tool is manufactured after a few months. Then, the experiments of the SR bonnet on an aspheric surface will be done. However, from the results above, the SR bonnet still has a certain flexibility which makes the contact spot a standard circle rather than a point. It also can deliver different sizes of tool spots, which indicates that it has a certain flexibility. It still can conform to the aspheric surface, at least for a low gradient aspheric surface. This will be further proved in future papers.

Table 4 demonstrates the general comparison between different subaperture polishing tool types. However, we have to acknowledge that some characteristics may not agree with this general comparison for a specific tool. Compared to

these tool types, the SR bonnet inherits many advantages of the normal bonnet and also possesses a high removal rate. Hence, it has the potential to be an attractive polishing tool to enhance the efficiency when polishing large size optical mirrors.

6 Conclusion

The SR bonnet tool—a novel loose abrasive highly efficient deterministic polishing tool for optical elements—is presented in this paper. It inherits the advantages of the normal bonnet, which means it not only has a certain flexibility, but also has a quite high stiffness. It can be used in the same way as the normal bonnet. Like the normal bonnet, the SR bonnet's TIF is also Gaussian-like and has a much higher material removal rate. The uniform removal test of the SR bonnet demonstrates a quite high uniformity of removal. Its ability to generate both TIFs with excellent uniformity and a high-accuracy surface texture indicates that it can be used both in fine polishing and corrective polishing. In the prepolishing test, the SR bonnet again demonstrates high-efficiency material removal, and it will be an attractive solution for the prepolishing process on optical elements, especially for large-sized ones. Considering its flexibility, it also has potential to be used in polishing aspheric surfaces and this will be demonstrated in future reports.

Acknowledgments

We appreciate the invaluable expert comments and advice on the manuscript from all anonymous reviewers. This work was financially supported by major national science and technology projects (Grant No. 2013ZX04006011-206).

References

1. P. R. Hall, "Role of asphericity on optical design," *Proc. SPIE* **1320**, 384–393 (1990).
2. R. A. Jones, "Computer control for grinding and polishing," *Photon. Spectra*, 34–39 (1963).
3. R. E. Wagner and R. R. Shannon, "Fabrication of aspherics using a mathematical model for material removal," *Appl. Opt.* **13**(7), 1683–1689 (1974).
4. R. A. Jones, "Computer-controlled polishing of telescope mirror segments," *Opt. Eng.* **22**(2), 236–240 (1983).
5. D. D. Walker et al., "The 'Precessions' tooling for polishing and figuring flat, spherical and aspheric surfaces," *Opt. Express* **11**(8), 958–964 (2003).
6. H. M. Pollicove, E. M. Fess, and J. M. Schoen, "Deterministic manufacturing processes for precision optical surfaces," *Proc. SPIE* **5078**, 90–96 (2003).

7. J. H. Burge et al., "Fabrication and testing of 1.4-m convex off-axis aspheric optical surfaces," *Proc. SPIE* **7426**, 74260L1 (2009).
8. R. A. Jones, "Fabrication of a large, thin, off-axis aspheric mirror," *Opt. Eng.* **33**(12), 4067–4075 (1994).
9. L. N. Allen, "Progress in ion figuring large optics," *Proc. SPIE* **2428**, 237–247 (1995).
10. T. W. Drueding et al., "Ion beam figuring of small optical components," *Opt. Eng.* **34**(12), 3565–3571 (1995).
11. O. W. Föhnle, H. van Brug, and H. Frankena, "Fluid jet polishing of optical surfaces," *Appl. Opt.* **37**(28), 6771–6773 (1998).
12. V. W. Kordonski et al., "Magnetorheological-suspension-based finishing technology," *Proc. SPIE* **3326**, 527–535 (1998).
13. R. G. Bingham et al., "A novel automated process for aspheric surfaces," *Proc. SPIE* **4093**, 445–448 (2000).
14. D. D. Walker et al., "The first aspheric form and texture results from a production machine embodying the precessions process," *Proc. SPIE* **4451**, 267–276 (2000).
15. D. D. Walker et al., "Use of the 'Precessions'™ process for prepolishing and correcting 2D & 21/2D form," *Opt. Express* **14**(24), 11787–11795 (2006).
16. G. Yu, H. Li, and D. D. Walker, "Removal of mid spatial-frequency features in mirror segments," *J. Eur. Opt. Soc. Rap. Pub.* **6**, 11044 (2011).
17. C. R. Dunn and D. D. Walker, "Pseudo-random tool paths for CNC sub-aperture polishing and other applications," *Opt. Express* **16**(23), 18942–18949 (2008).
18. D. D. Walker et al., "Edges in CNC polishing: from mirror-segments towards semiconductors, Paper 1: edges on processing the global surface," *Opt. Express* **20**(18), 19787–19798 (2012).
19. H. Li et al., "Edge control in CNC polishing, paper 2: simulation and validation of tool influence functions on edges," *Opt. Express* **21**(1), 370–381 (2013).
20. D. D. Walker et al., "New results from the precessions polishing process scaled to larger sizes," *Proc. SPIE* **5494**, 71–80 (2004).
21. A. Beaucamp et al., "Finishing of Optical moulds to $\lambda/20$ by automated corrective polishing," *Ann. CIRP* **60**(1), 3750378 (2011).
22. D. D. Walker et al., "Recent developments of precessions polishing for larger components and free-form surfaces," *Proc. SPIE* **5523**, 281–289 (2004).
23. C. F. Cheung et al., "Modelling and simulation of structure surface generation using computer controlled ultra-precision polishing," *Precis. Eng.* **35**(4), 574–590 (2011).
24. D. D. Walker et al., "New results extending the Precessions process to smoothing ground aspheres and producing freeform parts," *Proc. SPIE* **5869**, 79–87 (2005).
25. D. D. Walker et al., "A quantitative comparison of three grolishing techniques for the Precessions process," *Proc. SPIE* **6671**, 66711H (2007).
26. D. W. Kim and S. W. Kim, "Static tool influence function for fabrication simulation of hexagonal mirror segments for extremely large telescopes," *Opt. Express* **13**(3), 910–917 (2005).
27. D. D. Walker et al., "Precessions aspheric polishing: new results from the development programme," *Proc. SPIE* **5180**, 15–28 (2003).
28. D. D. Walker et al., "The precessions polishing and hybrid grolishing process-implementation in a novel 1.2 m capacity machine tool," in *Proc. to the Laser Metrology and Machine Performance VII*, pp. 99–108 (2007).
29. D. W. Kim and J. H. Burge, "Rigid conformal polishing tool using non-linear visco-elastic effect," *Opt. Express* **18**(3), 2242–2257 (2010).
30. T. Arnold et al., "Ultra-precision surface finishing by ion beam and plasma jet techniques-status and outlook," *Nucl. Instrum. Methods Phys. Res.* **616**(2–3), 147–156 (2010).
31. W. Liao et al., "Microscopic morphology evolution during ion beam smoothing of Zerodur surfaces," *Opt. Express* **22**(1), 377–386 (2014).
32. M. Schinhaerl et al., "Advanced techniques for computer-controlled polishing," *Proc. SPIE* **7060**, 70600Q1 (2012).
33. S. M. Booi, "Fluid jet polishing—possibilities and limitations of a new fabrication technique," PhD Dissertation, Delft University of Technology (2003).

Chunjin Wang is a graduate student specializing in measurement technology and instrumentation and is now a PhD candidate in the Micro-nano Manufacturing and Measuring Laboratory, Department of Mechanical and Electrical Engineering, Xiamen University, China. His research interests include advanced optical fabrication, aspherical surface fabrication, bonnet polishing and its machine tool design, as well as computer-controlled optical surfacing techniques.

Wei Yang is now an assistant professor in the Micro-nano Manufacturing and Measuring Laboratory, Department of Mechanical and Electrical Engineering, Xiamen University. His research interests include high-precision manufacturing and measuring, particularly for optical elements.

Biographies for the other authors are not available.